Eurasian Journal of Physics and Functional Materials

Volume 9 | Number 3

Article 7

Pages: 1 - 1

2025

Activation of luminescent-dosimetric properties of a single-crystal lithium-doped potassium chloride matrix.

Sh. Sagimbayeva
K. Zhubanov Aktobe Regional University, Aktobe 030000, Kazakhstan.

A. Kenzhebayeva
K. Zhubanov Aktobe Regional University, Aktobe 030000, Kazakhstan., akenzhebayeva@zhubanov.edu.kz

A. Istlyaup
K. Zhubanov Aktobe Regional University, Aktobe 030000, Kazakhstan.

K. Shunkeyev
K. Zhubanov Aktobe Regional University, Aktobe 030000, Kazakhstan.

Recommended Citation

Sagimbayeva, Sh.; Kenzhebayeva, A.; Istlyaup, A.; and Shunkeyev, K. (2025) "Activation of luminescent-dosimetric properties of a single-crystal lithium-doped potassium chloride matrix.," *Eurasian Journal of Physics and Functional Materials*: Vol. 9: No. 3, Article 7.
DOI: https://doi.org/10.69912/2616-8537.1257

ORIGINAL STUDY

Activation of Luminescent-dosimetric Properties of a Single-crystal Lithium-doped Potassium Chloride Matrix

Shynar Sagimbayeva, Adelya Kenzhebayeva*, Assel Istlyaup, Kuanyshbek Shunkeyev

K. Zhubanov Aktobe Regional University, Aktobe 030000, Kazakhstan

Abstract

An intense high-temperature thermally stimulated luminescence (TSL) dosimetric peak at 505 K was discovered in KCl:Li crystals. At a lithium concentration of 400 ppm, its integral light yield ($\eta_{KCl:Li}$) associated with the TSL_{505K} peak exceeds the integral light yield (η_{KCl}) of the TSL_{400K} peak, characteristic of pure KCl crystals, by more than two orders of magnitude. Furthermore, it significantly surpasses the corresponding light yield of the conventional dosimetric crystal LiF:Mg,Ti ($\eta_{LiF:Mg,Ti}$). The integral light yield (η), defined as the area under the TSL curve, was determined by integrating the intensity signals over the temperature range of 300−650 K.

Long-term storage of KCl:Li crystals leads to a decrease in the integral light yield of the TSL peaks at 400 K and 505 K, which is attributed to the reduction of lithium ions from regular cationic lattice sites ($Li^{+}_{K^{+}}$). Regeneration of the sample by annealing at 650 °C restores the maximum TSL light yield.

Estimates of the tetrahedral void radius (r_t), the radius of the "window" (r_x) into the tetrahedral void, and the lithium ion radius (r_{Li^+}) indicate that the lithium ion can easily move through interstitial sites in the KCl matrix after leaving the regular lattice site ($Li^{+}_{K^{+}}$), since $r_{Li^+} < r_x < r_t$.

The observed effect of enhancement in the integral TSL light yield at 505 K in KCl:Li crystals is promising for the development of new dosimetric detectors based on alkali halide crystals (AHCs) doped with light homologous cations (Li^+), which are capable of localizing mobile electronic excitations and radiation defects.

Keywords: Alkali halide crystal (AHC), Integral thermally stimulated luminescence (TSL), High-temperature TSL peak, Radiation defect formation, Recombination luminescence

1. Introduction

In alkali halide crystals (AHCs), it is possible to investigate two competing processes that influence the luminescence yield: the radiative channel, responsible for light emission, and the non-radiative channel, associated with radiation-induced defect formation. Both processes originate from the decay of self-trapped excitons (STEs) [1,2].

This underpins ongoing efforts to develop next-generation scintillators [3−6] and to improve the fundamental understanding of conventional scintillators [7−12], with the goal of identifying promising materials for advanced imaging systems, such as computerized and positron emission tomography with high spatial resolution.

Parallel to these developments, there is a significant focus on the search for a wide range of dosimetric materials for ionizing radiation dose monitoring. A prominent example is thermoluminescent dosimeters (TLDs) based on LiF single crystals. Owing to their tissue-equivalent properties, LiF-based TLDs have found widespread application in radiobiology and radiation therapy [13−15], as well as biological shielding from neutron radiation in nuclear reactors [16−20].

LiF crystals doped with cationic impurities, such as LiF:Mg,Ti and LiF:Mg,Cu,P, are used as dosimetric detectors (TLD-100 and TLD-700H, respectively) for

Received 8 July 2025; revised 27 August 2025; accepted 30 August 2025.
Available online 7 October 2025

* Corresponding author at: 34 A. Moldagulova ave., Aktobe 030000, Kazakhstan.
E-mail address: akenzhebayeva@zhubanov.edu.kz (A. Kenzhebayeva).

https://doi.org/10.69912/2616-8537.1257

measuring ionizing radiation doses up to 10 Gy. In these detectors, the primary dosimetric signals are high-temperature thermally stimulated luminescence (HTSL) peaks with maxima at 473 K (TLD-100) and 490 K (TLD-700H) [16–27].

The established fundamental relaxation channels of electronic excitations in AHCs provide a reliable framework for further exploration of the physical principles governing modern thermoluminescent dosimetric detectors. In this context, investigation of the mechanisms of HTSL in the well-characterized KCl single-crystal matrix doped with lithium ions (KCl:Li) is appropriate and parallels the use of LiF:Mg,Ti crystals in commercial TLD applications. In the single-crystal KCl:Li matrix, lithium ions occupy regular cationic lattice sites ($Li^{+}_{K^{+}}$), maintaining charge neutrality with respect to the host lattice. At the same time, due to the substantial (nearly twofold) difference in ionic radii between K^{+} and Li^{+}, a potential field is introduced, and it effectively traps low-energy electronic excitations (excitons, electrons, holes, and mobile radiation-induced defects) [20,28–36].

In the present study, a novel HTSL peak with a maximum at 505 K (TSL_{505K}) has been identified in KCl:Li crystals. We present comprehensive experimental data demonstrating the influence of key factors on the TSL_{505K} peak: (i) the lithium ion concentration (up to 400 ppm), (ii) the relaxation time, which leads to instability in the displaced KCl:Li system, and (iii) thermal quenching (650 °C), which facilitates the regeneration of the distorted crystal lattice. Furthermore, we provide stoichiometric justification for the decomposition, recovery, and enhancement of radiation defect formation, as evidenced by the TSL_{505K} peak intensity.

2. Material and methods

Single crystals of KCl and KCl:Li were grown at the Institute of Physics, University of Tartu, Estonia, using the Stockbarger method in evacuated quartz ampoules following a specialized purification procedure [36,37], which consists of the following sequential stages:

(i) The powdered KCl raw material was vacuum-dried at 80–90 °C for 24–48 h to remove oxygen-containing impurities (hydroxyl groups). Effective purification required keeping the raw material temperature below 100 °C to avoid oxide formation, which would complicate decontamination from oxygen-based species. According to absorption spectroscopy data, the residual OH content after drying was below 0.1 ppm—three orders of magnitude lower than in the initial material.

(ii) The KCl melt was treated with gaseous chlorine to remove homologous anions, primarily bromide. Chlorine ions replaced bromide ions in the melt, enabling their removal in gaseous form. Spectroscopic analysis confirmed that the content of residual anionic and cationic homologues was reduced to ~1.5 ppm—two orders of magnitude lower than in the initial material.

(iii) Multiple recrystallization, i.e. “zone melting” of the raw KCl based on differences in the incorporation coefficients (k) of impurities during crystallization. This method is particularly effective for impurities with $k \ll 1$.

As a result of this multi-step purification process, highly pure KCl crystals with impurity ion concentrations in the range of 0.1–1.5 ppm were obtained.

KCl:Li crystals were grown using purified KCl (devoid of OH and Br), with the addition of vacuum-dried LiCl powder. Because of the high hygroscopicity of LiCl, weighing and mixing of the KCl:LiCl powder mixture were carried out in a glove box under an inert gas atmosphere. The added amount of LiCl to the growth charge (inside the quartz ampoule) was within the limits of 10^4 ppm. Taking into account the lithium incorporation coefficient ($k = 0.03$) into the KCl lattice, the estimated maximum lithium ion concentration ($Li^{+}_{K^{+}}$) in KCl:Li was approximately 400 ppm. This estimation aligns with data obtained from flame photometric analysis. The notation $Li^{+}_{K^{+}}$ indicates that a lithium ion occupies a regular cationic site in place of a potassium ion in the KCl:Li crystal lattice.

Prior to experimental use, the crystals were annealed in an inert gas atmosphere using a Programix TX 25 electric muffle furnace (Ugin-Dentaire). The programmed annealing cycle included heating at a rate of 15 °C/min to a target temperature of 650 °C, holding at this temperature for 15 min, followed by rapid cooling to room temperature on a quartz substrate [36,37].

The irradiation dose calibration of the TLD-100 dosimeter (LiF:Mg,Ti was carried out at the National Center of Expertise and Certification of the Republic of Kazakhstan. An X-ray irradiation dose of 1.0 Gy (±0.1 Gy) was selected as optimal for all crystals in terms of sensitivity to TSL peak detection. All samples, identical in size ($3.0 \times 3.0 \times 1.0$ mm^3), were irradiated at room temperature (295 K) using the same experimental geometry for exposure to ionizing radiation and featuring a standardized heating area of the Harshaw Model 3500 reader.

The linear heating rate was strictly maintained at 5 K/s for all samples in compliance with the above-mentioned important experimental parameters over the wide temperature range of 300–850 K using a Harshaw 3500 TSL dosimetry system [37]. The

experiment was controlled via a computer connected to the Harshaw 3500 unit through an RS-232 port, using the WinREMS (Windows Radiation Evaluation and Management System) software. The integral light yield (η), characterized by the area under the TSL curve, was calculated by integrating the luminescence intensity signals over the 300–800 K temperature range. The integration was performed in MathCad after exporting the experimental TSL data of the crystals.

3. Results and discussion

3.1. High-temperature TSL of KCl and KCl:Li crystals

The physical mechanism underlying TSL is based on recombination luminescence that arises from interactions between the products of thermal dissociation of halogen-related radiation defects generated under ionising radiation exposure [28,34,37–39]. The light yield of TSL is directly dependent on the concentration of such defects, underscoring the importance of investigating mechanisms that promote the efficient formation of high-temperature radiation defects.

It is now established that in AHCs, the mobility of self-trapped holes (*V*K-centers) becomes significant within a certain temperature range, above which the probability of recombination luminescence increases due to the interaction of non-relaxed holes with immobile radiation defects [28,29,39].

Analysis of the thermal stability of self-trapped holes [28,29] shows that for halide anions with the same ionic radii (e.g. $r_a^-(\mathrm{Cl}_a^-) = 1.81$ Å), the decreasing radii of cations in the AHC lattice, following the trend $r_c^+(\mathrm{Li}_c^+) < r_c^+(\mathrm{Na}_c^+) < r_c^+(\mathrm{K}_c^+) < r_c^+(\mathrm{Rb}_c^+)$, determine the decrease in the self-trapping temperature of *V*K-centers. For example, in LiCl, the thermal destruction of *V*K-centers (and hence the TSL peak) occurs at 120 K [30]; in NaCl, at 168 K [28,29,38]; in KCl, at 208 K [28,38,40]; and in RbCl, at 240 K [31].

Thus, low-temperature integral TSL (85 K → 300 K) typically originates from the recombination of delocalised hole-type radiation defects—of the V_K-family (V_K, V_F, V_KA, V_KAA)—with electronic *F*-centers that consist of an electron localised at an anion vacancy, $(\upsilon_a^+ e^-)$ [2,32,36–38].

Above room temperature, stable radiation defects in AHCs are complementary pairs $V_2 = (X_3^-)_{aca}$- and $F = (\upsilon_a^+ e^-)$-centers, whose maximal thermal annealing is accompanied by luminescence in the range of 370–420 K [2,32,36–40].

Experimental data analysis reveals that for cations with identical classical ionic radii (e.g. $r_c^+(\mathrm{K}_c^+) = 1.33$ Å), the increase in the destruction temperature of $V_2 = (X_3^-)_{aca}$-centers is governed by decreasing ionic radii of AHC matrix anions across the series: $r_a^-(\mathrm{I}_a^-) < r_a^-(\mathrm{Br}_a^-) < r_a^-(\mathrm{Cl}_a^-)$. Accordingly, the maximum TSL peaks associated with V_2-center destruction are observed at Refs. [2,32,36,39,40]: 370 K in KI, 380 K in KBr, 400 K in KCl, 420 K in NaCl. Minor peak shifts (5–7 K) may occur due to variables such as irradiation temperature, dose, heating rate, and crystal size (optimally 2 × 2 × 0.7 mm^3).

The thermal dissociation of V_2-centers in AHCs results in the formation of mobile and positively charged V_K-, V_F-and *H*-centers [37,40], which are highly likely to recombine with *F*-centres and generate TSL peaks at 370–420 K.

Fig. 1 presents results of registration of high-temperature peaks of TSL for pure KCl (curve 1) and KCl:Li crystals (curves 2–5 with increasing lithium concentrations), all irradiated with X-rays at room temperature under identical conditions.

In pure KCl (curve 1, highlighted in blue), a well-defined TSL peak at 400 K corresponds to the V_2-centre, typically described as a $(\mathrm{Cl}_3^-)_{aca}$ molecule occupying two anionic (*a*) and one cationic (*c*) sites in the lattice [2,28,34–36]. Additionally, weak unresolved high-temperature peaks were observed, presumably due to uncontrolled impurities or aggregated halogen-related defects.

In KCl:Li crystals with low lithium content (100 ppm), the activation of $V_2 = (\mathrm{Cl}_3^-)_{aca}$-centers is enhanced compared to undoped KCl, and a new TSL peak emerges at 505 K (curve 2, Fig. 1). With increasing lithium concentration (100 → 400 ppm), a linear growth in the intensity of the 505 K TSL peak is observed (curves 2–5 and inset *a* of Fig. 1), indicating its potential as a dosimetric signal for ionising radiation detection. Notably, the peak maximum remains consistently at 505 K, an essential criterion for the selection of robust luminescent dosimeters. Temperature determination of TSL peaks was achieved with an accuracy of ±2 K, based on multiple experimental data sets using optimally sized crystals (2 × 2 × 0.7 mm^3).

In KCl:Li crystals, within the temperature range of 350–460 K, several unresolved TSL bands were observed at 400 K, 422 K, 434 K, and 452 K. The intensities of these peaks are an order of magnitude greater than those in undoped KCl (compare curves 1 and 5). These peaks are attributed to halogen-related centers similar to well-known $V_2 = (\mathrm{Cl}_3^-)_{aca}$, with more advanced aggregation. Fig. 1 clearly demonstrates that the incorporation of lithium ions into the KCl lattice promotes the efficient formation of both intrinsic halogen radiation defects (350–460 K) and lithium-sensitive defects (505 K).

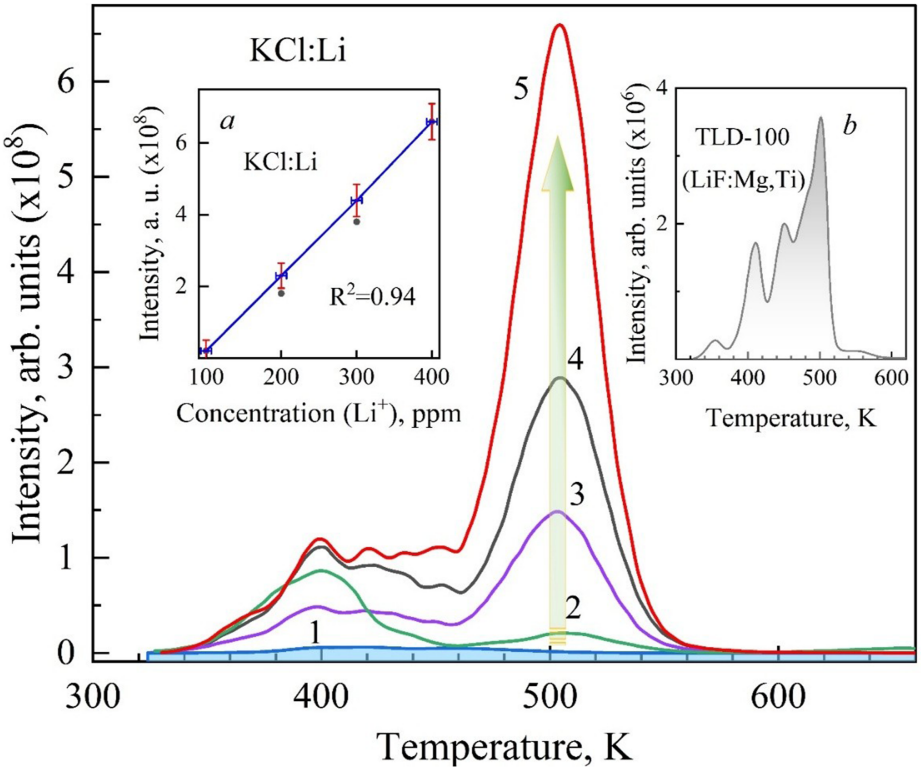

Fig. 1. Integral thermally stimulated luminescence of KCl (curve 1, undoped) and KCl:Li crystals with increasing lithium concentrations: 100 ppm (curve 2), 200 ppm (curve 3), 300 ppm (curve 4), and 400 ppm (curve 5); measured at room temperature following X-ray irradiation using RUP-120 (with W-anticathode), operating at 3 mA and 100 kV with a dose exposure of 1.0 Gy (±0.1). The arrow indicates the enhancement of the TSL_{505K} peak. The error in TSL registration depends on the intensity of the emitted signal and is estimated as follows: at 10^2–9.2 %; at 10^4–2.1 %; at 10^6–1.3 %; and in the range 10^7–10^8 – less than 1.0 %.
Insets: (a) Dependence of the TSL_{505K} peak intensity on lithium ion concentration in KCl:Li crystals, $R^2 = 0.94$; (b) TSL of a LiF:Mg, Ti crystal (TLD-100).

The overall light yield (η) of the dosimetric TSL peak at 505 K, as a function of lithium ion concentration, was quantified using two approaches: by evaluating the peak intensity (I_{max}) and by calculating the area under the TSL curve (S). Both methods confirmed a linear dependence with high accuracy (see Table 1).

For relative intensity-based estimation, the peak intensity of the TSL_{505K} peak in undoped KCl was taken as a reference value (I_a), while the peak intensities for KCl:Li crystals with 100 ppm, 200 ppm, 300 ppm, and 400 ppm of lithium were denoted as I_b, I_c, I_d and I_d, respectively, where $n = b, c, d, e$ (see inset *a* of Fig. 1 and Table 1).

For area-based estimation, the area under the TSL_{505K} peak in undoped KCl was used as the reference value (S_a), and the areas for the KCl:Li crystals with 100 ppm, 200 ppm, 300 ppm, and 400 ppm were designated as S_b, S_c, S_d и S_d, respectively.

Table 1. Integrated light yield of the TSL peak at 505 K in KCl and KCl:Li crystals with increasing lithium ion concentrations (100 → 400 ppm), estimated by both the maximum intensity ($\eta \sim f(I_{max})$) and the area under the TSL curve ($\eta \sim f(S)$).

Crystals	$\eta \sim f(I_{max})$ ($\times 10^8$)	$\eta \sim f(I_n/I_a)$	$\eta \sim S = \int_{T_1}^{T_2} I(T)dT$ ($\times 10^9$)	$\eta \sim f\left(\frac{S_n}{S_a}\right)$
1	2	3	4	5
KCl	$I_a = 0.03$	1	$S_a = 0.07$	1
KCl:Li (100 ppm)	$I_b = 0.3$	10	$S_b = 0.7$	10
KCl:Li (200 ppm)	$I_c = 1.5$	50	$S_c = 3.4$	48.5
KCl:Li (300 ppm)	$I_d = 2.7$	90	$S_d = 7.1$	101.4
KCl:Li (400 ppm)	$I_e = 6.5$	217	$S_e = 17.7$	252.8

The error in determining the integrated area under the TSL curve is expressed as $S_{TSL} = (S_{TSL} \pm \Delta) \times 10^9$, where S denotes the mean value, and Δ varies within (0.1 ÷ 0.5), depending on lithium concentration.

As shown in Table 1, the increase of η, both in terms of peak intensity (column 3) and area under the curve (column 5), exhibits a clear linear trend with increasing lithium ion concentration in KCl:Li crystals. The discrete step-wise growth coefficients repeat with high consistency, demonstrating 10-, 50-, 90-, and 217-fold increases relative to the undoped KCl crystal.

The activation energy (E_a) of the TSL_{505K} peak for the KCl:Li(400 ppm) crystal, calculated from experimental data using the Lushchik formula [31, 37 and references therein], was found to be in the range of 1.1–1.3 eV, which is characteristic of the migration of both anionic and cationic vacancies during the high-temperature destruction of halogen aggregates.

These results experimentally confirm that the observed increase in intensity of the high-temperature TSL_{505K} peak is directly attributed to the presence of lithium ions that act as a stimulator for the efficient formation of halogen-related radiation defects.

The key finding for the KCl:Li crystal system is the experimentally established linear dependence of the TSL peak intensity at 505 K on lithium ion concentration (illustrated in the inset *a* of Fig. 1). This promising trend supports the rationale for systematic investigations aimed at identifying novel dosimetric TSL peaks.

Further analysis of the TSL peak intensities reveals that the dosimetric TSL_{505K} peak in KCl:Li ($I_{max} = 6.5 \cdot 10^8$) has integral light yield more than 2 orders of magnitude higher compared to the TSL_{400K} peak in undoped KCl ($I_{max} = 3 \cdot 10^6$), as shown in column 2 of Table 1. A similar result is observed when evaluating the integrated light yield by the area under the TSL curve ($\eta \sim S = \int_{T_1}^{T_2} I(T)dT$), with KCl:Li ($17.7 \cdot 10^9$) significantly surpassing undoped KCl ($7 \cdot 10^7$), as shown in columns 4 and 5 of Table 1.

Analysis of the integral light yield of the dosimetric TSL peaks of KCl:Li crystals (TSL_{505K} peak, $I_{max} = 6.5 \cdot 10^8$, $S = 17.7 \cdot 10^9$, see Table 1 and inset *a* Fig. 1) and LiF:Mg, Ti (TSL_{495K} peak, $I_{max} = 3.8 \cdot 10^6$, $S = 1.0 \cdot 10^8$, inset *b* in Fig. 1) demonstrates that, at a lithium concentration of 400 ppm in KCl:Li, the dosimetric light sum significantly exceeds that of LiF:Mg,Ti.

In comparative analysis of TSL light yield, the primary parameter considered is the area under the TSL glow curve, as it provides a more accurate and stable measure than peak intensity. For example, of the TSL_{505K} peak in KCl:Li crystals or the TSL_{495K} peak in LiF:Mg,Ti crystals. It has been established that a shift in the TSL peak position by up to ±5 K has a negligible effect on the integrated area under the glow curve (S). This observation was taken into account in the analysis of the TSL light yield $\eta \sim f(S)$.

This substantial enhancement in the integrated TSL light yield at 505 K highlights the strong potential of KCl:Li crystals as a foundation for developing next-generation dosimetric detectors. Based on the study of HTSL peaks in KCl:Li crystals, we propose a plausible luminescence mechanism for radiation-induced defect centers: a recombinative reassembly process in the potential field of the impurity ion (Li^+), involving non-relaxed holes (h) and free electrons (e) released during thermal dissociation of halogen aggregates [9,12,30, 33,36].

3.2. Studies of KCl:Li crystal relaxation by TSL method

In the crystalline lattice of KCl:Li, the lithium impurity ion, bearing the same positive charge, substitutes for the host potassium ion (K^+), i.e. it occupies the cationic lattice site of potassium ($Li^+_{K^+}$). Owing to the significant difference in classical ionic radii—0.68 Å for lithium versus 1.33 Å for potassium—a potential field arises within the KCl:Li matrix, capable of efficiently trapping both radiation-induced defects [29,29,31] and low-energy electronic excitations [9,12,31,32].

According to Ref. [32], high-temperature (above 300 K) radiation-induced defects in the KCl matrix are halogen-related formations. The most elementary among these are $V_2 = (Cl_3^-)_{aca}$-centers, which occupy one cationic (c) and two anionic (a) sites in the crystal lattice. They exhibit an absorption band with a maximum at approximately 5.2 eV, which is annealed at 400 K (see also Fig. 1 in the 400 K region).

In KCl:Li(400 ppm), the an intense emergence of TSL_{505K} peak is accompanied by a slower increase in the intensity of the TSL_{400K}, attributed to the thermal decay of $V_2 = (Cl_3^-)_{aca}$-centers.

This observation suggests that the presence of lithium in the KCl lattice enhances the formation of radiation-induced defects. As reported in [32, see also [295] there], this occurs due to the interaction of two interstitial halogen atoms in the field of a lithium ion, according to the following reaction:

$$Li_c^+ \left(Cl_2^-\right)_a + \left(Cl_2^-\right)_a \rightarrow \left(Cl_3^-\right)_{aca} Li_i^+ Cl_i^- \quad \text{or} \quad \left(Cl_3^-\right)_{aca} \ldots\ldots Li_i^+ Cl_i^- . \tag{1}$$

In KCl crystals, lithium-associated formations are denoted analogously to $V_2 = (Cl_3^-)_{aca}$-centers as $V_{2A} = (Cl_3^-)_{aca}Li_i^+Cl_i^-$-centers, which exhibit absorption maxima at 4.9 eV [32]. Based on the reaction above, halogen complexes may form either in close proximity to lithium ions ($(Cl_3^-)_{aca}Li_i^+Cl_i^-$) or at a distance of several lattice constants ($(Cl_3^-)_{aca} \ldots\ldots Li_i^+Cl_i^-$). Depending on

the degree of correlation between lithium and halogen species, TSL_{400K} (V_2) and TSL $_{505K}$ (V_{2A}). peaks may arise. At high temperatures, it is also plausible that larger aggregates (n) of halogen and lithium formations could be formed, i.e. $(Cl_3^-)\,Li_n^+$.

Relaxation processes in KCl:Li(400 ppm), which tend to destabilize the lattice, are accompanied by a marked decline in the efficiency of halogen-related radiation defect formation. This concerns both own $(Cl_3^-)_{aca}$-centers (TSL_{400K} peak) and lithium-related $(Cl_3^-)_{aca}\,Li_i^+Cl_i^-$-centers ($TSL_{505K}$ peak), as illustrated in logarithmic coordinates in Fig. 2.

According to Fig. 2, from the freshly quenched state (curve 1) to full relaxation (curves 2 and 3), the intensities of the TSL peaks at 400 K and 505 K diminish by more than three orders of magnitude.

First of all, in zone-refined KCl crystals (curve 4), the V_2-center is predominantly observed (TSL_{400K} peak). Notably, no trace of lithium ions is detected, as no TSL signal is observed at 505 K, the region corresponding to the thermal annealing of V_{2A}-centers (curve 4 in Fig. 2).

Numerous experiments have shown that, following annealing, the KCl:Li crystals exhibit nearly complete recovery of TSL intensity (curve 5, Fig. 2). Therefore, prior to any measurements, each sample was mandatorily annealed according to the procedure described in Section 2. This thermal treatment not only eliminates residual absorbed dose (non-annealed radiation defects), but more importantly, based on experimental evidence, it restores the crystalline lattice of KCl:Li. The result of annealing is the reintegration of lithium ions into regular cationic sites and the re-establishment of a homogeneous distribution of lithium throughout the KCl matrix.

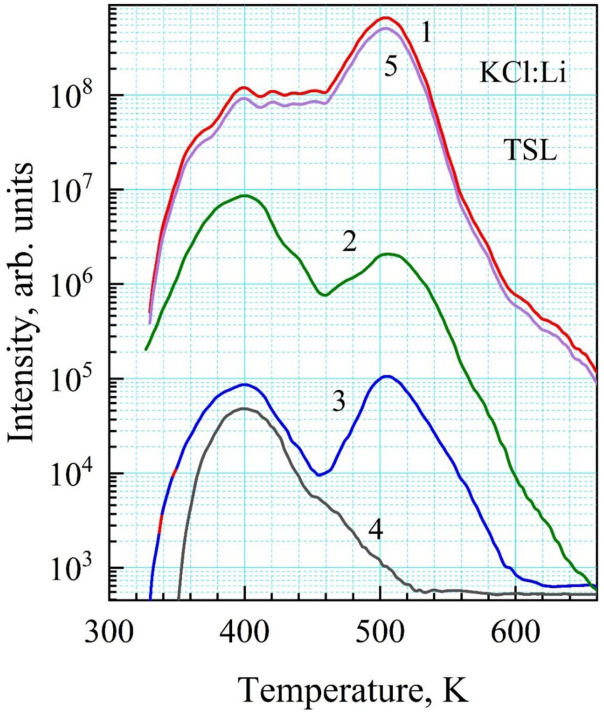

Fig. 2. TSL curves of KCl:Li(400 ppm) crystals in logarithmic coordinates: curve 1 — freshly quenched crystal; curve 2 — same crystal after one month of relaxation; curve 3 — after more than three months of relaxation; curve 4 — zone-refined KCl crystal, curve 5 — the previously disintegrated KCl:Li crystal after quenching. X-ray irradiation was conducted at room temperature using RUP-120 (W-anticathode), operating at 3 mA and 100 kV, with a dose exposure of 0.5 ÷ 1.0 Gy.

It is well known that the efficiency of radiation defect formation in KCl crystals at temperatures where *H*-centers (interstitial chlorine atoms) become mobile ($T > 55$ K) is determined by their stabilization efficiency. The primary complementary to *F*-centers defects stabilizing *H*-centers are Cl_3^--centers, which form via mutual interaction of two *H*-centers according to the reaction:

$$(Cl_2^-)_a + (Cl_2^-)_a \rightarrow (Cl_3^-)_{aca}K_i^-Cl_i^- \qquad (2)$$

According to Reaction (2), a linear trihalide radiation-induced defect is formed occupying one cationic (*c*) and two anionic (*a*) lattice sites [30,31]. In KCl:Li crystals, this reaction is expected to occur with greater efficiency if the *H*-centres associate in the vicinity of lithium ions. Due to the significantly smaller radius of the lithium ion compared to the potassium ion, local lattice rearrangement can facilitate the formation of $(Cl_3^-)_{aca}$-centers.

Reference [30] provides detailed data on the influence of lithium impurities on the radiation-induced formation of Cl_3^--centers in KCl and KBr crystals within the 80–300 K range. It was shown that increasing the lithium concentration and irradiation temperature up to 300 K leads to an order-of-magnitude increase in intrinsic Cl_3^--centers relative to undoped crystals. The enhanced efficiency of complex halide defect formation is presumably due to Li^+ migration through interstitial positions, creating cationic vacancies where Cl_3^--centers subsequently form.

Complex trihalide radiation-induced defects are known to originate from interactions between mobile halogen atoms occupying regular lattice sites [30,31]. Consequently, the detection of vacancy dipole complexes suggests that they may significantly enhance the overall radiation defect formation process, as the formation of halide centers occupying one cationic and two anionic sites is energetically favorable. Therefore, assessing the efficiency of radiation defect formation in the field of such vacancy dipole complexes is a logical continuation of this research.

From the attenuation of the characteristic indicators—the TSL peaks at 400 K and 505 K—it is evident that long-term storage of KCl:Li crystals leads to the

ejection of lithium dopant ions from their regular cationic lattice sites (see curves 1–3 in Fig. 2), likely followed by the formation of their interstitial clusters.

The primary cause of the structural instability of the KCl:Li system is the off-center positioning of lithium ions within the cationic sub lattice of KCl. This phenomenon was first confirmed through the identification of H_A (Li_c^+)-centers [30,31,34,35]. In KCl:Li crystals, these centers represent interstitial chlorine atoms stabilized in the fields of lithium ions ($Li_{K^+}^+$) occupying cationic sites of the regular lattice, i.e. K^+.

3.3. Stoichiometric rationale for the instability of KCl:Li crystals

Subsequent large-scale experimental studies of absorption and luminescence properties over a wide temperature range in AHCs doped with light homologous cations confirmed the presence of instability effect, exemplified by the KCl:Na crystal system. Fig. 2 demonstrates that the highly sensitive TSL technique enables detailed monitoring of the degradation process of the KCl:Li crystal structure via the intensity of the TSL_{505K} peak. This approach is significantly more sensitive than absorption spectroscopy, which was previously applied to investigate structural instability in KCl:Na crystals [37]. During the relaxation of the crystal at room temperature, lithium impurity ions are displaced from regular cationic lattice sites, as evidenced by the decrease in the TSL_{505K} peak intensity over time (Fig. 2).

It is likely that, upon leaving the cationic site, lithium ions migrate into tetrahedral interstitial voids through so-called “windows” formed by three neighboring halogen ions, as illustrated in Fig. 3. To validate this hypothesis, two parameters must be taken into account: (i) the radius of the “window” (r_x), defined by the configuration of three adjacent halide ions along the <111> direction; and (ii) the radius of the tetrahedral void (r_t), located at the intersection of the spatial diagonals of the cubic unit cell (see Fig. 3a).

One of the key criteria governing the unhindered migration of light impurity cations (Li^+, Na^+) in the AHC lattice is that the ionic radius of the impurity ion (r_{Li^+}) must be smaller than both the window radius ($r_{Li^+} < r_x$ and $r_{Na^+} < r_x$) and the radius of the tetrahedral void ($r_{Li^+} < r_t$ and $r_{Na^+} < r_t$).

r_t is determined, according to Fig. 3a, by the following formula:

$$r_t = \frac{1}{2}\left[\frac{\sqrt{3}a}{2} - r_a^- - r_c^+\right]. \quad (3)$$

Here, a is the lattice constant, r_a^- is the ionic radius of the anion, and r_c^+ is the ionic radius of the cation.

r_x along the <111> direction from Fig. 3b is calculated using the following formula:

$$r_x = \frac{a}{\sqrt{6}} - r_a^-. \quad (4)$$

Table 2 presents calculated values of r_t and r_x, along with their ratios to the ionic radii of lithium, sodium, and potassium ions $\left(\frac{r_t}{r_c^+(M_A^+)}; \frac{r_x}{r_c^+(M_A^+)}\right)$ for NaCl, KCl and RbCl crystals, where $r_c^+(M_A^+)$ denotes ionic radii of impurity cations, i.e. $M_A^+ = Li^+$, Na^+, K^+.

The numbers in parentheses reflect values computed using physical radii of the constituent ions, while those without parentheses are based on classical ionic radii

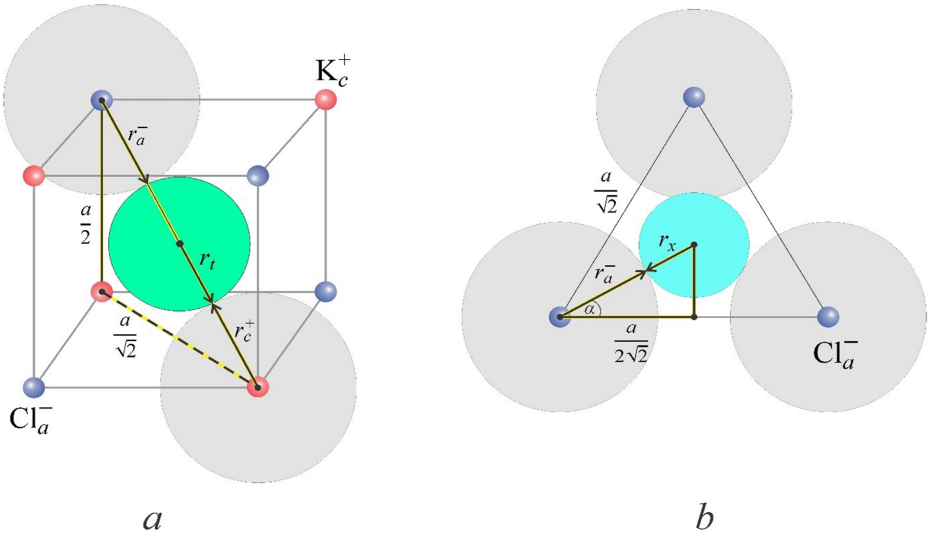

Fig. 3. Schematic models: (a) for determining the tetrahedral void radius r_t; (b) for calculating the window radius r_x along the <111> direction for NaCl, KCl, and RbCl crystals. Relative proportions of r_a^-, r_t and r_x are preserved in the diagram.

Table 2. Calculated values of tetrahedral void radii (r_t) and window radii (r_x), and their ratios to the radii of impurity cations $\left(\frac{r_x}{r_c^+(M_A^+)}\right)$ *and* $\left(\frac{r_t}{r_c^+(M_A^+)}\right)$ *for selected crystals.*

Crystals	a, Å [41]	r_t, Å	r_x, Å	$r_c^+(M_A^+)$, Å [41]		$\frac{r_t}{r_c^+(M_A^+)}$	$\frac{r_x}{r_c^+(M_A^+)}$
1	2	3	4	5		6	7
NaCl:Li	5.64 (5.66)	1.05 (1.04)	0.58 (0.59)	Li^+	0.68 (0.9)	**1.54 (1.15)**	0.85 (0.65)
KCl:Li	6.29 (6.38)	1.14 (1.17)	0.75 (0.93)	Li^+	0.68 (0.9)	**1.67 (1.17)**	**1.1 (1.03)**
KCl:Na				Na^+	0.98 (1.16)	**1.16 (1.0)**	0.76 (0.8)
RbCl:Li	6.58 (6.66)	1.2 (1.22)	0.87 (1.04)	Li^+	0.68 (0.9)	**1.76 (1.35)**	**1.27 (1.15)**
RbCl:Na				Na^+	0.98 (1.16)	**1.22 (1.05)**	0.88 (0.89)
RbCl:K				K^+	1.33 (1.52)	0.9 (0.8)	0.65 (0.68)

Note: the values of a, r_x and r_t are given in parentheses based on the physical ionic radii of cations and anions.
Bold numbers indicate values of calculated parameters greater than one (>1.0).

obtained from lattice constants. It is known [41] that classical ionic radii derived from lattice constants are less accurate than physical ionic radii, which are determined via X-ray measurements of electron density distributions in crystals.

Fig. 3a and b presents scaled unit cells preserving the proportionality of physical radii between anions and cations that can be very close. For instance, in KCl the ratio $[r(Cl^-)/r(K^+)] = 1.09$. This geometrical consistency renders the model suitable for evaluating r_x and r_t, the physical meaning of which is assessing feasibility of lithium ion migration into interstitial sites in the KCl matrices (also extendable to NaCl and RbCl, as detailed in Table 2).

Overall, the physical interpretation derived from Table 2 is largely independent of whether classical or physical radii are used. According to the presented numerical analysis, the following conclusions can be drawn:

1. In KCl:Li and RbCl:Li crystals, lithium ions can move freely, since their radii are smaller than both r_t and r_x ($r_{Li^+} < r_t$ and $r_{Li^+} < r_x$), i.e. $\frac{r_t}{r_c} > 1$ и $\frac{r_x}{r_c} > 1$ (see columns 3, 5, 6, and 7 of Table 2).
2. In NaCl:Li, KCl:Na, and RbCl:Na crystals, lithium and sodium ions can reside in interstitial lattice voids, as $\frac{r_t}{r_c^+(M_A^+)} > 1.0$ (see column 6 of Table 2). However, some activation barrier exists due to the impurity ion radius exceeding the "window" radius (see column 7 of Table 2), as indicated by $\frac{r_x}{r_c^+(M_A^+)} < 1.0$.

The experimentally observed instability effect of the KCl:Li crystalline system is supported by the calculated data confirming the possibility of lithium impurity ion (Li_c^+) migration to an interstitial site, i.e., a more energetically favorable configuration. These calculations (columns 6 and 7) also suggest that similar instability may occur in RbCl:Li and RbCl:Na crystals, as was previously reported for KCl:Na [38].

In general, the instability of mixed crystal systems can be evaluated based on the impurities' coefficient (k) of incorporation into the host lattice [32,40]. Analysis indicates that homologous cations of small radius ("light cations" – Li^+, Na^+) exhibit very low incorporation coefficients ($k \ll 1.0$) in AHCs. For example, in KCl:Na, $k_{Na_c^+}$ equals 0.3; in NaCl:Li and KCl:Li, $k_{Li_c^+}$ is as low as 0.03. These low incorporation coefficients likely explain the observed instability of the distorted crystalline systems.

The analysis shows that in KCl:Li crystals, the lower the lithium incorporation coefficient ($k_{Li_c^+} = 0.03$), the greater the ratio between the classical ionic radii of potassium and lithium ($r_{K^+}/r_{Li^+} = 1.95$). Based on the correlation between incorporation coefficients and ionic radii ratios, one can predict dynamics of instability in displaced KCl:Li crystals.

The fundamental nature of instability in the KCl:Li system lies in the fact that the small lithium ion (r_{Li^+}) can easily escape from the cationic lattice site ($Li_{K^+}^+$), passing through a narrow channel formed by three adjacent anions (r_x) and moving into the interstitial tetrahedral void (r_t), since $r_{Li^+} < r_x < r_t$.

According to the computed data, there are no geometric constraints preventing lithium ions from entering an interstitial position in the KCl lattice via the following mechanisms:

$$Li_c^+ \rightarrow Li_{ic}^+ \upsilon_c^- \text{ or } Li_c^+ \rightarrow Li_c^+ \ldots \upsilon_c^-. \quad (5)$$

$Li_{ic}^+ \upsilon_c^-$ denotes a partially occupied cationic site due to the significantly smaller ionic radius of Li^+ compared to K^+ (nearly twofold difference, see Table 2). The notation $Li_c^+ \ldots \upsilon_c^-$ refers to the formation of a dipole involving lithium ions migration into interstitial regions of the KCl lattice.

Reaction (3) is highly probable, considering that at room temperature, cationic vacancies, unlike anionic ones, exhibit high mobility [37]. The initial non-central position of the lithium ion within the cationic site of the

KCl crystal lattice [35], along with our identified stoichiometric condition ($r_{Li^+} < r_x < r_t$), arising from the comparatively small ionic radius of Li^+, provides a physically plausible mechanism for the displacement of lithium into a tetrahedral interstitial site. This relocation is considered a necessary condition for interpreting the instability of the KCl:Li crystalline system. According to Ref. [37], in undoped KCl crystals at low temperatures (293 K), the jump frequency of cation vacancies exceeds that of anion vacancies by a factor of more than 40. In crystals doped with lithium or sodium, this ratio increases by over a thousand times. Furthermore, ionic conductivity data reported in ([31], see also [295] there) confirm that, unlike in pure KCl, the cationic conductivity in KCl:Li crystals increases by an order of magnitude within the temperature range of 295 K→560 K. This enhancement is indicative of lithium ion mobility within the host KCl lattice.

From Table 2, it follows that a similar instability mechanism may be expected not only in KCl:Li crystals (see Section 3.2, Fig. 2), but also in RbCl:Li, RbCl:Na, and KCl:Na [36].

Given these facts, one can assume that instability is an inherent property of all AHCs doped with isoelectronic cations: the positive charge of the impurity ion retains it within the cationic lattice site, whereas dimensional compatibility facilitates its migration into an interstitial position. Therefore, the instability effect in KCl:Li crystals can be suppressed by thermal quenching (see Fig. 2, curve 5), which promotes the re-establishment of a homogeneous lithium distribution within the KCl matrix.

Thus, high-temperature quenching (650 °C) contributes to the regeneration of the KCl:Li crystal lattice, resulting in the reincorporation of lithium ions into cationic sites, as evidenced by the restored TSL intensities at 400 K and 505 K (curve 5 in Fig. 2). Quenching not only purges the dosimetric crystal of residual absorbed doses (i.e., unannealed radiation defects), but more importantly, as shown by the experimental data, almost entirely restores the mixed crystalline lattice structure. In this regard, it is recommended that all dosimetric crystals undergo thermal annealing prior to use. This pre-treatment serves not only to remove residual background radiation effects but also to regenerate and stabilize the crystal structure.

4. Conclusions

Experimental data on the registration of high-temperature TSL peaks demonstrate that the presence of light lithium ions (Li^+) in KCl:Li crystals initiates the appearance of a dosimetric TSL peak with a maximum at 505 K (TSL_{505K}).

Analysis of the integral light output (η) of TSL peaks in a KCl:Li crystal (400 ppm) shows that the TSL_{505K} peak, both in terms of intensity ($I_{max} = 6.5 \cdot 10^8$) and integrated area under the curve ($S = 17.7 \cdot 10^{10}$), exceeds by more than two orders of magnitude the corresponding TSL_{400K} peak of undoped KCl ($I_{max} = 3 \cdot 10^6$; $S = 7 \cdot 10^7$).

The Li^+ ion in the KCl crystal promotes the efficient formation of radiation-induced halogen defects (TSL_{505K} peak), which are structurally characterized as $(Cl_3^-)_{aca}$ $Li_i^+Cl_i^-$ centers that are formed via the interaction of mobile interstitial halogen atoms (*H*-centers) in the field of the dipole complex $Li_{ic}^+ \upsilon_c^-$, as described in Ref. [37], according to the following reaction:

$$Li_{ic}^+ \upsilon_c^- + \left(Cl_2^-\right)_a + \left(Cl_2^-\right)_a \rightarrow \left(Cl_3^-\right)_{aca} Li_i^+ Cl_i^- . \quad (6)$$

This process is analogous to the association of *H*-centers at regular lattice sites, but is energetically more favorable because the lithium ion has already been partially displaced from the cationic lattice site prior to the reaction ($Li_c^+ \rightarrow Li_{ic}^+ \upsilon_c^-$).

Estimates of the stoichiometric parameters of alkali metal chloride lattices also confirm the unobstructed migration of lithium ions through the interstitial sites of the KCl matrix, since the ionic radius of lithium (r_{Li^+}) is smaller than both the radius of the tetrahedral interstitial void and the radius of the "window" leading to it ($r_{Li^+} < r_x < r_t$).

Thus, a high-temperature dosimetric TSL_{505K} peak was identified in KCl:Li crystals, which warrants further investigation for the development of future luminescent dosimeters.

Funding

The research work has been funded by Science Committee of the Ministry of Science and Higher Education of the Republic of Kazakhstan (Grant No. AP26100001).

Conflicts of interest

The authors declare no conflict of interest.

Acknowledgment

The authors express their sincere gratitude to Professor D. Sergeyev for valuable insights during the analysis.

References

[1] K.S. Song, R.T. Williams, Self-Trapped Excitons, Springer Science & Business Media, 2013, https://doi.org/10.1007/978-3-642-85236-7. ISBN: 978-3-642-85236-7.

[2] C. Lushchik, A. Lushchik, Evolution of anion and cation excitons in alkali halide crystals, Phys. Solid State 60 (2018) 1487–1505, https://doi.org/10.1134/S1063783418080164.
[3] X. Li, J. Yu, Y. Fan, Y. Gao, G. Niu, Aggregation-induced emissive scintillators: a new Frontier for radiation detection and imaging, Nano-Micro. Lett. 17 (1) (2025) 160, https://doi.org/10.1007/s40820-025-01671-x.
[4] P. Mangthong, M. Kohout, C.S. Ponseca Jr., Z. Hubička, J. Kaewkhao, S. Kothan, et al., Hybrid detectors for high-energy radiation based on borosilicate glass scintillator doped with Gd^{3+} covered by photosensitive TiO2 layer, Radiat. Phys. Chem. 237 (2025) 113010, https://doi.org/10.1016/j.radphyschem.2025.113010.
[5] T. Wang, G. Zeng, Y.M. Yang, Z. Yang, T. Wang, H. Li, et al., Advances in metal halide perovskite scintillators for x-ray detection, Nano-Micro Lett 17 (1) (2025) 275, https://doi.org/10.1007/s40820-025-01772-7.
[6] L. Prouzová Procházková, F. Hájek, M. Buryi, Z. Remeš, V. Čuba, Radiation stability of nanocomposite scintillators, Radiat. Phys. Chem. 237 (2025) 112991, https://doi.org/10.1016/j.radphyschem.2025.112991.
[7] Y. Takizawa, et al., Growth of thallium-doped CsI/CsCl/KCl eutectics and their scintillation properties, Opt. Mater. X 15 (2022) 100159, https://doi.org/10.1016/j.omx.2022.100159.
[8] Y. Takizawa, et al., Large size growth of terbium doped BaCl2/NaCl/KCl eutectic for radiation imaging, Jpn J. Appl. Phys. 61 (SC) (2022) SC1009, https://doi.org/10.35848/1347-4065/ac3b23.
[9] K. Shunkeyev, A. Kenzhebayeva, A. Krasnikov, et al., Luminescence of bound excitons created near sodium impurity ions in KCl:Na single crystals, Opt. Mater. X 25 (2025) 100395, https://doi.org/10.1016/j.omx.2024.100395.
[10] K. Miyazaki, et al., Tl-concentration dependence of photoluminescence and scintillation properties in Tl-doped RbI single crystals, J. Mater. Sci. Mater. Electron. 33 (2022) 1–7, https://doi.org/10.1007/s10854-022-08996-y.
[11] K. Miyazaki, et al., Development of Tl-doped KI single crystal scintillators, Radiat. Phys. Chem. 207 (2023) 110820, https://doi.org/10.1016/j.radphyschem.2023.110820.
[12] K. Shunkeyev, A. Kenzhebayeva, S. Sagimbayeva, et al., Luminescence of CsI:Na crystal scintillator under synchrotron radiation excitation, J. Lumin. 284 (2025) 121308, https://doi.org/10.1016/j.jlumin.2025.121308.
[13] Y. Takizawa, et al., Growth and scintillation properties of Tl-doped CsI/KI/KCl ternary eutectics, J. Cryst. Growth 573 (2021) 126287, https://doi.org/10.1016/j.jcrysgro.2021.126287.
[14] Y. Takizawa, et al., Growth and scintillation properties of Tl-doped CsI/CsCl/NaCl ternary eutectic scintillators, Jpn J. Appl. Phys. 60 (2021) SBBK01, https://doi.org/10.35848/1347-4065/abcdab.
[15] A. Blomgren, A. Tartas, P.K. Meher, S. Silverstein, A. Wojcik, B. Brzozowska, Home-made low-cost dosemeter for photon dose measurements in radiobiological experiments and for education in the field of radiation sciences, Radiat. Environ. Biophys. 63 (3) (2024) 395–404, https://doi.org/10.1007/s00411-024-01076-1.
[16] D. Guerreiro, J. Saraiva, M. Borges, J. Sampaio, L. Peralta, Development of a plastic scintillating optical fibers array dosimeter for radiobiology, J. Instrum. 19 (5) (2024) P05006, https://doi.org/10.1088/1748-0221/19/05/P05006.
[17] L.A. DeWerd, K. Kunugi, Accurate dosimetry for radiobiology, Int. J. Radiat. Oncol. Biol. Phys. 111 (5) (2021) e75–e81, https://doi.org/10.1016/j.ijrobp.2021.09.002.
[18] N. Salah, P.D. Sahare, A.A. Rupasov, Thermoluminescence of nanocrystalline LiF:Mg, Cu, P. J Lumin 124 (2007) 357–364, https://doi.org/10.1016/j.jlumin.2006.04.004.
[19] Y.S. Horowitz, Linearisation of the dose response of composite peak 5 in LiF:Mg,Ti by post-irradiation photon excitation, Phys Med Biol 69 (2024), https://doi.org/10.1088/1361-6560/ad8298.
[20] S. Lee, J. Lee, G. Kim, S.J. Ye, Estimating 10B and 14N doses using a pair of LiF-Based TLD-600 and TLD-700 as an alternative to gold activation method, Nucl. Instrum. Methods Phys. Res. A 1050 (2023) 168141, https://doi.org/10.1016/j.nima.2023.168141.
[21] Y.S. Horowitz, L. Oster, I. Eliyahu, The Saga of the thermoluminescence (TL) mechanisms and dosimetric characteristics of LiF:Mg,Ti (TLD-100), J. Lumin. 214 (2019) 116527, https://doi.org/10.1016/j.jlumin.2019.116527.
[22] M. Behmadi, S. Mohammadi, M.E. Ravari, et al., Neutron dosimetry with a pair of TLDs for the elekta precise medical linac and the evaluation of optimum moderator thickness for the conversion of fast to thermal neutrons, Nucl. Eng. Technol. 56 (2024) 753–761, https://doi.org/10.1016/j.net.2023.11.014.
[23] C. Iliaskou, M. Gainey, B. Thomann, et al., Development of a TLD-100 based set up for in vivo dosimetry in Intraoperative Electron Beam Radiation Therapy (IOERT): an experimental and clinical evaluation, Z. Med. Phys. (2025), https://doi.org/10.1016/j.zemedi.2025.04.007.
[24] E. Saeedian, M. Shakerian, A.Z. Sanayei, et al., Thermoluminescence dosimetry in small animal digital radiography, the dose to animals, and their adopters, Radioprotection 60 (1) (2025) 57–64, https://doi.org/10.1051/radiopro/2024035.
[25] M.E.V. Larsson, P.I. Jonasson, P.S. Apell, et al., Evaluation of novel radiation protection devices during radiologically guided interventions, CVIR Endovasc. 7 (1) (2024) 18, https://doi.org/10.1186/s42155-024-00430-0.
[26] E.B. Jumpeno, R. Anggraeni, M. Muharani, et al., Dose response of Hp(0.07) on TLD-700 and TLD-900 based ring dosimeters to the Sr-90 exposure, At. Indones. 50 (3) (2024) 267–271, https://doi.org/10.55981/AIJ.2024.1425.
[27] M. Alizadeh, M. Mohseni, B. Farhood, et al., Thermoluminescent characteristics of GR200, TLD-700H and TLD-100 for low dose measurement: linearity, repeatability, dose rate and photon energy dependence, J. Biomed. Phys. Eng. 12 (2) (2022) 111–116, https://doi.org/10.31661/jbpe.v0i0.1247.
[28] D.G. Schoemaker, Hyperfine components of V_K centers, Phys. Rev. B 7 (2) (1973) 786–801, https://doi.org/10.1103/PhysRevB.7.786.
[29] T.G. Castner, W. Kanzig, The electronic structure of V-centers, J. Phys. Chem. Solid. 3 (1957) 178–195, https://doi.org/10.1016/0022-3697(57)90023-9.
[30] K. Shunkeyev, Z. Aimaganbetova, L. Myasnikova, et al., Mechanisms of radiation defect formation in KCl crystals under the influence of local and plastic deformation, Nucl. Instrum. Methods Phys. Res. B 509 (2021) 7–11, https://doi.org/10.1016/j.nimb.2021.10.010.
[31] C. Lushchik, A. Lushchik, Decay of Electronic Excitations with Defect Formation in Solids, Nauka, 1989. ISBN: 978-5-02-014026-4.
[32] J. Aluker, D. Lusis, S. Chernov, Electronic excitations and radioluminescence of alkali halide crystals, Riga, Zinatne (1979) 252 (In Russian).
[33] K. Shunkeyev, A. Tilep, S. Sagimbayeva, et al., The enhancement of exciton-like luminescence in KCl single crystals under local and uniaxial elastic lattice deformation, Nucl. Instrum. Methods Phys. Res. B 528 (2022) 20–26, https://doi.org/10.1016/j.nimb.2022.08.002.
[34] D. Schoemaker, J.L. Kolopus, Electron paramagnetic resonance optical and absorption studies of the $V_1(Li^+)$ center in KCl:Li^+, Phys. Rev. B 2 (4) (1970) 114–1159, https://doi.org/10.1103/PhysRevB.2.1148.
[35] D. Schoemaker, E.L. Yasaitis, Reorientation motions of the $H_A(Li^+)$ center in KCl:Li^+, Phys. Rev. B 5 (12) (1972) 4970–4986, https://doi.org/10.1103/PhysRevB.5.4970.
[36] K. Shunkeyev, A. Tilep, S. Sagimbayeva, et al., The effect of instability of KCl:Na single crystals, Crystals 13 (2023), https://doi.org/10.3390/cryst13020364.
[37] K. Shunkeyev, S. Sagimbayeva, A. Kenzhebayeva, Z. Serikkaliyeva, The nature of high-temperature peaks of thermally stimulated luminescence in NaCl:Li and KCl:Na crystals, Crystals 15 (1) (2025) 67, https://doi.org/10.3390/cryst15010067.
[38] F.J. Keller, R.B. Murray, M.M. Abraham, R.A. Weeks, Preferential thermal reorientation of V_K centers in potassium chloride,

Phys. Rev. 154 (3) (1967) 812−816, https://doi.org/10.1103/PhysRev.154.812.
[39] K. Shunkeyev, L. Myasnikova, A. Barmina, et al., The thermostimulated luminescence of radiation defects in KCl, KBr and KI crystals at elastic and plastic deformation, J. Phys. Conf. Ser. 830 (2017) 012138, https://doi.org/10.1088/1742-6596/830/1/012138.
[40] A.A. Elango, T.N. Nurakhmetov, Structure and generation mechanism of Br centres in x-rayed KBr, Phys. Status Solidi. B 78 (1976) 529−5336, https://doi.org/10.1002/pssb.2220780211.
[41] B.K. Vainshtein, V.M. Fridkin, V.L. Indenbom, Modern Crystallography 2: Structure of Crystals, 3rd ed., Springer-Verlag Berlin Heidelberg, 2000 https://doi.org/10.1007/978-3-642-57254-8. ISBN: 978-3-642-57254-8.